NASA TECHNICAL NOTE

NASA TN D-4501

A LIGHTING STRATEGY FOR
LUNAR ORBITER MISSION DESIGN

by Friedrich O. Huck

Langley Research Center

Langley Station, Hampton, Va.

NATIONAL AERONAUTICS AND SPACE ADMINISTRATION • WASHINGTON, D. C. • MAY 1968

A LIGHTING STRATEGY FOR LUNAR ORBITER MISSION DESIGN

By Friedrich O. Huck

Langley Research Center
Langley Station, Hampton, Va.

CONTENTS

A LIGHTING STRATEGY FOR LUNAR ORBITER MISSION DESIGN

By Friedrich O. Huck
Langley Research Center

SUMMARY

An analysis is presented which relates quality of lunar photographs to Lunar Orbiter trajectory. Furthermore, since several parameters which affect picture quality are uncertain, a strategy is developed which optimizes confidence levels in detecting specific lunar surface detail.

This strategy is illustrated by examining Lunar Orbiter's capability to reveal small obstacles in the form of right-circular cones which have lunar reflective properties. Results show that the smallest lunar detail can be detected at high phase angles (angle between incident light and camera) and long exposure times; however, the effects of variances in lunar reflectance, vehicle trajectory, and image smear result in higher levels of confidence in the detection of larger detail at lower phase angles and shorter film exposures.

INTRODUCTION

The prime objective of the Lunar Orbiter project is to obtain topographic information regarding various lunar areas to assess their suitability for use as Apollo landing sites. Since photographic quality in revealing small obstacles which would be hazardous to the Lunar Module varies strongly with vehicle trajectory and film exposure, a criterion is needed for the selection of these parameters to optimize detail detectability.

Several measures of photographic quality have been established to define Lunar Orbiter's capability to aid in the Apollo program. This paper presents an analysis which relates these measures of picture quality to viewing geometry and camera shutter speeds. Furthermore, this paper considers the uncertainties which exist in lunar reflective properties, vehicle trajectory, and camera system operation by developing a lighting strategy for securing maximum levels of confidence in the detection of specific lunar features as a function of viewing geometry and camera shutter speeds.

An image signal-to-noise ratio of lunar features is selected as an appropriate assessment of picture quality because it includes the effects of lunar reflection, viewing geometry, and camera characteristics and because it is a measure of the information

content in the photographic image. Because of the high cost of obtaining closeup photographs of the lunar surface, it is desirable that these photographs contain maximum information about small detail. Thus, a convenient measure of Lunar Orbiter's capability to reveal small depressions and proturberances has been established in terms of the detectability of right-circular cones which are near the limits of the camera system resolution. This measure of picture quality is introduced in this paper to illustrate the proposed lighting strategy.

Because the detection of small detail is of primary interest, results of this analysis are given for the high-resolution camera system and an expected vehicle perilune of 46 kilometers. Under these conditions, Lunar Orbiter's vertical viewing geometry can be expressed as a function of phase angle alone, where phase angle is defined as the angle between incident light and camera axis. And, because lunar targets near the limits of the system resolution are considered, the system may be linearized without introducing significant errors.

While these factors simplify computations, the basic analysis is not restricted to them, but represents a general approach to the prediction of picture quality and optimum viewing geometry for the photography of moon and planets by a spacecraft camera.

SYMBOLS

A   area: on lunar surface, meter^2; on film image, millimeter^2

B   brightness, meter-candles

d   cone diameter: on lunar surface, meters; on film image, millimeters

E   exposure, meter-candle-seconds

f_n focal ratio or "f-number"

F   spread function

g   phase angle, degrees

G   modulation transfer function (MTF)

h   height, kilometers

k   fundamental spatial frequency component of cone model, lines/millimeter

2

K	solar constant, meter-candles
L	linear operator
m,n	dummy variables
N	root-mean-square (rms) noise
O	lunar object
p	probability density function
s	smear, 1σ value of Gaussian smear distribution: on lunar surface, meters; on film image, millimeters
S	signal
S/N	signal-to-rms-noise ratio (hereinafter referred to as signal-to-noise ratio)
t	exposure time, sec
T	film transmission
u,v	spatial frequency, lines per millimeter
x,y,z	spatial dimensions: on lunar surface, meters; on film image, millimeters
β	lunar slope
γ	confidence level
δ	difference between actual mean value of minimum detectable cone diameter and its estimate
Γ	nonlinear operator
θ	angle, degrees
$\vec{\lambda}$	vector parameter set representing spatial dimension or spatial frequency

μ actual mean value

$\vec{\xi}$ vector parameter set containing all variables which affect lighting strategy

ρ lunar albedo

σ standard or rms deviation of a Gaussian distribution

τ static lens transmission

$\Phi(\ )$ photometric function

$< \ >$ expected value

Subscripts:

a   aperture

b   background

c   film readout and communication subsystem

D   film density

d   cone diameter

e   effective

f   film

i   image

l lens

max   maximum

min   minimum

p   peak

4

q   dark

r   bright

s   smear

T   film transmission

ANALYSIS

Object Detectability Threshold

Signal analysis.- The most general description of the purpose of a camera is perhaps that it is to give information about an object. If it is required to extract all the information that is implicit in the resulting image regardless of the possible complexity of the interpretation, the quality of an image is most appropriately assessed by its signal-to-noise ratio (ref. 1). Accordingly, an image signal-to-noise ratio of lunar features is derived to predict picture quality. Since the detection of small objects is of primary interest, it is convenient to give this ratio for signals near the limits of system resolution. For this purpose, a simplified block diagram of the Lunar Orbiter photographic system is given in figure 1. The properties of lunar reflection (refs. 2 to 5) and the assessment of optical images in the presence of signal degradation and noise (refs. 1, 6, 7, and 8) are discussed in this analysis only to the extent to which the proposed lighting strategy and hence photographic mission design is affected.

All system elements, except film response to exposure, can be considered linear (ref. 9); film conversion of exposure to transmission can be treated approximately as linear only if very low contrast objects are considered. It is convenient here to define $\vec{\lambda}$ as a vector parameter set representing spatial dimension or frequency variables and $\vec{\xi}$ as a vector parameter set containing all variables which affect lighting strategy, and, furthermore, to define L as a linear operator and Γ as a nonlinear operator.

For an object description $O(\vec{\lambda};\beta)$ with spatial dimensions or frequencies $\vec{\lambda}$ and slope β, the photometric function of the lunar surface yields a brightness variation which can be expressed as (ref. 2)

$$\Delta B(\vec{\lambda};\beta,g) = K\rho \; \Delta\Phi(\vec{\lambda};\beta,g) \tag{1}$$

where

K   solar constant at moon surface

ρ full-moon albedo or reflectance coefficient for normal incidence and emission

$\Phi(\beta,g)$ surface photometric function normalized such that $\Phi(O,O) \equiv 1$

This brightness variation is a function of viewing geometry. For the Lunar Orbiter's vertical photography, viewing geometry may be expressed as a function of phase angle g as defined within a plane in figure 2(a). Brightness contrast as a function of a more general viewing geometry is given in reference 10.

      Exposure variations at the spacecraft camera focal plane are related to brightness by (ref. 2)

$$\Delta E\left(\vec{\lambda}_i;\beta,g,t\right) = \frac{\tau t}{4f_n^2}\,\Delta B\left(\vec{\lambda};\beta,g\right) \tag{2}$$

where

t   exposure time

f_n camera lens f-number

τ static optical transmittance

Lunar object dimensions $\vec{\lambda}$ and film image dimensions $\vec{\lambda}_i$ are related by camera lens focal length and vehicle altitude over the object. Exposure variations may, therefore, for a given lens be written as a function of vehicle height h as $\Delta E(\vec{\lambda};\beta,g,t,h)$.

      Because of degrading effects due to image smear s and lens-film characteristics, the actual film exposure variation is

$$\Delta E_f\left(\vec{\lambda};\vec{\xi}\right) = L_{l,f}\left(\vec{\lambda}\right) L_s\left(\vec{\lambda};s\right)\left\{\Delta E\left(\vec{\lambda};\beta,g,t,h\right)\right\} \tag{3}$$

where $\vec{\xi} = \beta,g,t,h,s$. This equation may be rewritten as

$$\Delta E_f\left(\vec{\lambda};\vec{\xi}\right) = L_{l,f,s}\left(\vec{\lambda};s\right)\left\{\Delta E\left(\vec{\lambda};\beta,g,t,h\right)\right\} \tag{4}$$

where

$$L_{l,f,s}\left(\vec{\lambda};s\right) = L_{l,f}\left(\vec{\lambda}\right) L_s\left(\vec{\lambda};s\right) \tag{5}$$

      If the vector parameter set $\vec{\lambda}$ is defined as a spatial dimension set (x,y), then the operation of $L_{l,f,s}(x,y;s)$ on the input signal $\Delta E(x,y;\beta,g,t,h)$ becomes the convolution integral

$$\Delta E_f\left(x,y;\vec{\xi}\right) = \int_{-\infty}^{\infty} \int_{-\infty}^{\infty} F_{l,f,s}(x-x',y-y';s)\,\Delta E(x',y';\beta,g,t,h)dx'\,dy' \tag{6}$$

6

where $F_{l,f,s}(x,y;s)$ is the combined lens-film and image smear spread function. If, however, the vector parameter set $\vec{x}$ is defined as a spatial frequency set (u,v), then $L_{l,f,s}(u,v;s)$ indicates multiplication, and equation (4) can be written as

$$\Delta E_f\left(u,v;\vec{\xi}\right) = G_{l,f,s}(u,v;s)\,\Delta E(u,v;\beta,g,t,h) \tag{7}$$

where $G_{l,f,s}(u,v;s)$ is the combined lens-film and image smear modulation transfer function (MTF). Spread function and MTF are related by the Fourier transform pair

$$G(u,v) = \int_{-\infty}^{\infty} \int_{-\infty}^{\infty} F(x,y)\, e^{-i2\pi(ux+vy)}\, dx\, dy \tag{8}$$

$$F(x,y) = \int_{-\infty}^{\infty} \int_{-\infty}^{\infty} G(u,v)\, e^{i2\pi(ux+vy)}\, du\, dv \tag{9}$$

Once film exposure is determined, the resulting film transmission can be evaluated from the film characteristic curve; this is depicted by using the nonlinear operator Γ_f, so that

$$\Delta T\left(\vec{x};\vec{\xi}\right) = \Gamma_f\left(\vec{\xi}\right)\left\{\Delta E\left(\vec{x};\vec{\xi}\right)\right\} \tag{10}$$

The signal passes then from the film to the film readout and communications link which are combined here into one block. The output signal is related to film transmission variations by the linear operator $L_c\left(\vec{x}\right)$, as given by

$$S\left(\vec{x};\vec{\xi}\right) = L_c\left(\vec{x}\right)\left\{\Delta T\left(\vec{x};\vec{\xi}\right)\right\} \tag{11}$$

which, again, indicates convolution in the spatial dimension domain and multiplication in the spatial frequency domain.

Combining equations (4), (10), and (11) and being careful not to disturb the correct order of operation with respect to the nonlinear operator gives the output signal in terms of the input exposure as follows:

$$S\left(\vec{x};\vec{\xi}\right) = L_c\left(\vec{x}\right)\Gamma_f\left(\vec{\xi}\right)L_{l,f,s}\left(\vec{x};s\right)\left\{\Delta E\left(\vec{x};\beta,g,t,h\right)\right\} \tag{12}$$

When scenes near the system resolution limit, yielding images of low contrast, or scenes which have low contrast are considered, the image distribution can be expressed as

$$S\left(x,y;\vec{\xi}\right) = \int_{-\infty}^{\infty} \int_{-\infty}^{\infty} \Delta E(u,v;\beta,g,t,h)\, G_{l,f,s,c}(u,v;s)\frac{\Delta T}{\Delta E}\left(E_b\right)e^{i2\pi(ux+vy)}\, du\, dv \tag{13}$$

where the linear operators $L_c(\vec{x})$ and $L_{l,f,s}(\vec{x};s)$ are replaced by the total system MTF $G_{l,f,s,c}(u,v;s)$, and the nonlinear operator $\Gamma_f(\vec{\xi})$ is replaced by the linearized film response $\frac{\Delta T}{\Delta E}(E_b)$. It may be noted that film response now becomes a function of the background exposure E_b.

Noise analysis.- All system noise sources are assumed to be "white," statistically independent, and represented by a Gaussian process. The total rms system noise is grouped for the present purpose into exposure-dependent film granularity noise and exposure-independent communications noise. A detailed discussion of all system noise sources is given in reference 9.

Film granularity noise is measured as the standard or rms deviation about the mean density and is commonly designated by σ_D. This rms value depends on the actual film graininess and the film scanning aperture area (ref. 11, p. 53) which is treated herein, in harmony with the discussion in the previous section, as part of the communication link. The rms fluctuations in film transmittance σ_T may be obtained from σ_D by the relation (ref. 12)

$$\sigma_T\left(E_b\right) = 2.3\overline{T}\left(E_b\right)\sigma_D\left(E_b\right) \tag{14}$$

where $\overline{T}$ is the average film transmission.

Noise in the communication link can be expressed in terms of an equivalent value σ_c at the system output, and it can be root sum squared with film transmission noise to yield a total rms noise as given by

$$\sigma\left(E_b\right) = \left[\sigma_T^2\left(E_b\right) + \sigma_c^2\right]^{1/2} \tag{15}$$

But noise content in an image depends not only on system noise sources and MTF, it depends also on the signal image area. This is simply because the larger the image area is, the more samples are obtained by the readout aperture as it scans across the film. The number of independent samples n that may be obtained from an image area A_i by an aperture area A_a is A_i/A_a. According to the Central Limit Theorem (ref. 13), the mean of a sample of size n has a standard deviation of $\sigma/\sqrt{n}$ if σ is the population deviation. The standard deviation from the mean value of an image area larger than the scanning aperture area is, therefore,

$$N\left(E_b\right) = \frac{\sigma\left(E_b\right)}{\sqrt{A_i/A_a}} \tag{16}$$

Signal-to-noise ratio.- Combining equations (13) and (16) gives an image signal-to-noise ratio for targets near the system detectability threshold as follows:

8

$$\frac{S}{N}\left(x,y;\vec{\xi}\right) = \frac{\Delta T/\Delta E}{\sigma}\left(E_b\right)\sqrt{\frac{A_i}{A_a}} \int_{-\infty}^{\infty}\int_{-\infty}^{\infty} \Delta E(u,v;\beta,g,t,h)\, G_{l,f,s,c}(u,v;s)e^{i2\pi(ux+vy)}du\,dv \qquad (17)$$

with exposure and frequency dependent system characteristics separated.

Object detection thresholds depend, of course, not only on image signal-to-noise ratios but also on the process of image interpretation, and become, therefore, a quantity of some arbitrariness. Detection thresholds have, nevertheless, been established. From an experimental study on the detection and identification of geometrical shapes, such as right-circular cones, in a simulated lunar environment (ref. 5) the following rule evolved: An object may be detected if its film image peak-to-peak signal-to-noise ratio is above 3 and identified if its size is about three times as large as needed for its detection. This signal-to-noise ratio detection threshold may be slightly optimistic in applications to actual lunar photographs, because the photo interpreters had been told the exact location of the test targets in the photographs. In evaluating photographic image quality, Schade (ref. 14) found that small image elements can be detected on a uniform background if their signal-to-noise ratio is about 3 to 4. Another study on imaging systems and human vision by Rose (ref. 15) indicates a signal-to-noise ratio of 5 as the lower limit for object detectability through visual observation.

However, the importance of calculating object detectability does not lie solely in the absolute magnitudes of the results. It is the variation of these results as a function of mission controllable variables which allows optimization of detail detectability by mission design. Because the Lunar Orbiter Project Statement of Work specifies as a mission goal that a cone of 2-meter diameter and a base-to-height ratio of 4:1 shall result in an image peak-to-peak signal-to-noise ratio of 3, this ratio is used as effective cone detectability threshold.

Lighting Strategy

Whereas equation (17) presents a fundamental relationship for calculating target signal-to-noise ratio, uncertainty of its results prevails due to variations in film exposure, phase angle, vehicle height, image smear, and other factors. Film exposure variations are expected because of uncertainties in lunar reflective characteristics and photographic subsystem properties; phase angle and vehicle height variations are expected due to trajectory uncertainties, and image smear variations are expected due to uncertainties in velocity-over-height sensor errors and other image motions (ref. 16). Of these parameters, optimum lighting is most critically affected by variations in exposure and phase angle. Image smear influences lighting primarily through the selection of exposure speed; camera height has no effect, but changes in height during exposure will cause an image smear known as the zoom effect.

A well-founded basis for selecting a lighting strategy must weigh these uncertainties. The strategy proposed here optimizes confidence levels in the detection of specific surface features. To accomplish this, an estimate of the actual, but a priori unknown, mean value of the minimum detectable target feature is made and used to place confidence limits on the detection of specified target features as a function of phase angle and camera shutter speed. The proposed lighting strategy is, for convenience, discussed in terms of minimum detectable cone diameters. But the strategy is applicable equally well to any other type of target.

Expected value of minimum detectable cone diameter.- As stated in the introduction, the primary objective of the Lunar Orbiter project is to gather information on the detailed surface structure of various lunar areas. In particular, several (on the average about 10) potential Apollo landing sites are to be photographed during a mission. And several photographs (on the average about 16 frames, each containing a high- and medium-resolution picture) are taken of each site.

In designing a phase angle (trajectory) and camera shutter speed for taking n photographs of a site, it is desirable that the average value of the detectable cone diameters for these n pictures be minimized. This average value is defined as $\langle \mu_d \rangle = \frac{1}{n} \sum_{i=1}^{n} \mu_{di}$, where μ_{di} is the a priori unknown minimum detectable cone diameter for the ith picture. The best available estimator of this quantity is the expected value of $d_{min}(\vec{\xi})$, which may be written as (refs. 13 and 17)

$$\langle d_{min} \rangle = \int_{-\infty}^{\infty} d_{min}(\vec{\xi})\, p(\vec{\xi})\, d\vec{\xi} \tag{18}$$

This is a best estimate of $\langle \mu_d \rangle$ in the sense that $\langle d_{min} \rangle$ can be expected to occur most frequently. In general, $\langle d_{min} \rangle \neq d_{min}(\langle \vec{\xi} \rangle)$, where $\langle \vec{\xi} \rangle$ indicates the most likely values of $\vec{\xi}$; these quantities are equal only in a linear system. In the case at hand, the lunar photometric value varies nonlinearly with phase angle, and the film transmission varies nonlinearly with exposure.

From the viewpoint of designing spacecraft trajectory and camera shutter speed, it is not of primary interest to predict the actual mean value of the minimum detectable cone diameter but to predict an optimum trajectory and shutter speed. For this purpose, equation (18) may, for numerical computations, be stated in a simplified form as a function of only those parameters which affect lighting geometry most critically, namely, film exposure and phase angle. The influence of image smear on viewing geometry and shutter speed selection can be observed by repeating these calculations for probable amounts of smear. Even though it is still convenient to talk about an expected value of the minimum detectable cone diameter, it should be kept in mind, however, that the

calculated mean values and confidence limits are actually still a function of image smear, vehicle height, and other parameters which affect object detection.

With these considerations, equation (18) becomes

$$\langle d_{min} \rangle = \int_{-\infty}^{\infty} \int_{-\infty}^{\infty} d_{min}(E,g) \, p(E,g) dE \, dg \tag{19}$$

Confidence levels in detection of a specified cone diameter.- A fundamental goal of this paper may be stated as follows: If $\langle \mu_d \rangle$ is the actual, a priori unknown, mean value of the minimum detectable cone diameter of a finite number of pictures taken of a lunar area, and $\langle d_{min} \rangle$ is its estimated value, what confidence level (Conf.) γ can be placed on the difference $\langle \mu_d \rangle - \langle d_{min} \rangle$ being equal to or less than some specified value δ? This statement can be expressed in the form (refs. 13 and 17)

$$\text{Conf.}\left(\langle \mu_d \rangle - \langle d_{min} \rangle \leqq \delta\right) = \gamma \tag{20}$$

If the value δ is chosen in such a manner that $\langle d_{min} \rangle + \delta = d$, where d is a specified cone diameter, equation (20) may be rewritten as

$$\text{Conf.}\left(\langle \mu_d \rangle \leqq d\right) = \gamma \tag{21}$$

and read as the confidence level γ that the mean value of the actual minimum detectable cone diameter is less than or equal to some specified diameter. And the confidence level of this event is, in turn, equal to the probability (Prob.) that the estimated values of all parameters which affect $\langle \mu_d \rangle$ are favorable to this event — that is,

$$\text{Conf.}\left(\langle \mu_d \rangle \leqq d\right) = \text{Prob.}\left(\langle \vec{\xi}_{min} \rangle \leqq \vec{\xi} \leqq \langle \vec{\xi}_{max} \rangle\right) = \int_{\langle \vec{\xi}_{min} \rangle}^{\langle \vec{\xi}_{max} \rangle} p(\vec{\xi}) d\vec{\xi} \tag{22}$$

where the range of $\langle \vec{\xi}_{min} \rangle$ to $\langle \vec{\xi}_{max} \rangle$ includes all the estimated values of $\vec{\xi}$ for which $\langle \mu_d \rangle \leqq d$.

Again if only film exposure and phase angle variations are considered, equation (22) is rewritten as

$$\text{Conf.}\left(\langle \mu_d \rangle \leqq d\right) = \text{Prob.}\left(\langle E_{min} \rangle \leqq E \leqq \langle E_{max} \rangle; \langle g_{min} \rangle \leqq g \leqq \langle g_{max} \rangle\right)$$

$$= \int_{\langle g_{min} \rangle}^{\langle g_{max} \rangle} \int_{\langle E_{min} \rangle}^{\langle E_{max} \rangle} p(E,g) dE \, dg \tag{23}$$

11

In essence, this equation is a summation of all the probabilities of those combinations of exposure and phase angle which yield an average detectable cone diameter less than a specified value d.

AN APPLICATION OF THE LIGHTING STRATEGY

The effect of the proposed lighting strategy on the selection of an optimum viewing geometry for detecting small cones is illustrated in this section. For this purpose, an approximate expression is derived which enables rapid estimates of the minimum detectable cone diameter as a function of mission variables. It is convenient to perform all calculations at the airborne film output. Signal degradation resulting from the communication link may be neglected without introducing significant errors in the general conclusions drawn from these calculations. However, before this formula can be developed, some properties of the lunar surface, the target signature, and the Lunar Orbiter photographic subsystem must be introduced. Computer programs have been written to calculate the detectability of cones and other targets with more detail and rigor (refs. 9 and 18); however, their results are in close agreement with those obtained here. And, while it is believed meaningful to present major system characteristics to illustrate computations, it does not aid the purpose of this paper to discuss all the system details that have been considered in the computer programs.

Lunar, Cone, and System Properties

Viewing geometry and lunar reflectivity.- For the vertical photography of the Lunar Orbiter, viewing geometry and lunar slope can be defined in a plane as shown in figure 2(a). Lunar reflective characteristics and film exposure are related for this geometry by (ref. 2)

$$E(\beta,g,t) = \frac{K\rho t\tau}{4f_n^2} \Phi(\beta,g) \tag{24}$$

The nominal values of the given parameters, as well as their tolerances, are given in table I. Curves of the lunar photometric function based on work by Hapke (ref. 3) and Willingham (ref. 4) are shown in figure 3.

Exposure and phase angle probability variations are assumed to follow a Gaussian distribution. This is suggested by the fact that these variations depend on a number of independent occurrences of which many have already been assumed to follow this distribution (ref. 16).

Uncertainties in the parameters which determine film exposure are expressed as exposure variations and are root sum squared to yield an exposure tolerance. The

12

probability density function $p(E,g)$, as given in equations (19) and (23), can be represented, in general, by the product of $p(E/g)$ and $p(g)$. Though exposure is a function of phase angle, exposure uncertainty is not; hence, the form of the conditional probability density function $p(E/g)$ does not change with phase angle. Since exposure deviation is given as a percentage of its mean value, its probability density function is unsymmetric and changes with mean value. It is, therefore, convenient to express this density function in terms of log exposure in order that its shape be symmetric and not vary with changes in mean log exposure. A discrete approximation of the log exposure and phase angle probability density function is given in figure 4.

Lunar cone model.- The Lunar Orbiter Project Statement of Work has described among other goals a 26.6^O, 2-meter-diameter cone as a measure of small obstacle detectability. An approximate model of this target is used in this paper to calculate its minimum detectable diameter. This model is depicted in figure 2.

The value of the photometric function Φ and, hence, lunar reflection depends on phase angle g and lunar slope β. These angles are defined in figure 2(a) in a plane parallel to the incident sunlight and the light reflected toward the camera. Away from this plane, the effective lunar slope — that is, as lunar slope affects the photometric function — becomes a function of the angle θ which is defined in figure 2(b). An expression which relates the effective lunar slope to the angle θ is derived in the appendix.

Since cone sizes near the limits of system resolution are of interest, the value of target brightness contrast with background can be taken as an average value (ref. 10). The choice of average values to represent a more complex cone surface brightness distribution is not unrealistic because small details will be largely obscured. The average photometric value is calculated here separately over those regions of the image which are brighter than the background $\bar{\Phi}_r$ and those regions which are darker than the background $\bar{\Phi}_q$. Results are given in figure 5. The estimate of $\bar{\Phi}_q$ becomes increasingly conservative as phase angles rise above 67° because effects of shadow are not fully considered.

To obtain maximum signal-to-noise ratio for a deterministic signal in the presence of white noise, a filter should be matched to the signal (ref. 19). Correspondingly, an optimum scanning aperture would be matched to the cone model's film image. This is easier in theory than in practice. Hence, a mathematical aperture area is used which is representative of an actual densitometer; namely, two neighboring circular areas whose diameters are equal to the radius of the actual cone and whose centers are located along sunline. This is indicated in figure 2(c). It is convenient to consider this configuration as a cone model and assign the average photometric value for the bright and dark side of the cone to these areas.

The scaling factor between lunar object dimension and airborne film image for an expected vehicle perilune of 46 km and a lens focal length of 610 mm is 0.0132 mm on the film per meter on the lunar surface.

Photographic subsystem characteristics and image smear.- It was shown in deriving equation (17) that for a small signal analysis the photographic subsystem of the Lunar Orbiter can be grouped into a spatial frequency and an exposure-dependent transfer function and that the transfer function for smear can be combined with the frequency-dependent system characteristics.

Frequency-dependent system characteristics: Signal degradation due to frequency-dependent system characteristics depends primarily on the lens and film modulation transfer function which is shown in figure 6(a). Noise generated in the communication link is nevertheless included.

Image smear is assumed random since it is caused by a number of independent motions (ref. 16). Its effect can be predicted by use of the modulation transfer function (ref. 8) as given in figure 6(b). The curves shown are labeled by their standard deviation referred to the airborne film and the lunar surface for a vehicle perilune of 46 km. The combined lens and smear modulation transfer functions are shown in figure 6(c).

Exposure-dependent system characteristics: Film transmission and granularity noise are exposure dependent. Nominal characteristics of film transmission plotted against exposure are shown in figure 7(a). Film transmission noise σ_T and a root-sum-square (rss) value of this transmission noise and communication noise σ_c (corresponding to an expected peak-to-peak signal-to-noise ratio of 30 dB) is plotted in figure 7(b).

For small signal calculations, a film-sensitivity-to-rms-noise ratio is given in figure 7(c). Film sensitivity $\Delta T/\Delta E$ was calculated for an exposure change of 0.1 meter-candle-second because images near the limits of system resolution exhibit approximately this film exposure variation.

Scanning aperture: Scanning aperture size, which determines the amount of film transmission noise due to granularity, also determines the number of samples obtained from a given image area. While the Lunar Orbiter photographic subsystem uses a Gaussian spot, Eastman Kodak Co. (ref. 16) measures granularity using a circular aperture of 6.48-micron diameter, and it is also convenient to use this circular aperture here. It has been shown in appendix D of reference 9 that granularity noise measurements yield equal results for these two apertures if the diameter of the circular aperture is 4σ and σ is the standard deviation of the Gaussian spot.

Calculations

Minimum detectable cone diameter.- An approximate expression is now derived from equation (17) to enable rapid estimates of minimum detectable cone diameters as a function of mission variables. It is convenient, at first, to consider only the signal term.

The signal component of equation (17) is

$$S(x,y;g,t,s) = \frac{\Delta T}{\Delta E}\left(E_b\right) \int_{-\infty}^{\infty} \int_{-\infty}^{\infty} \Delta E(u,v;g,t)\, G_{l,f,s}(u,v;s) e^{i2\pi(ux+vy)} du\, dv \qquad (25)$$

where the film readout and communcations system MTF are omitted. This expression is no longer a function of the variables β and h since these variables have been specified previously by selecting a 26.6° cone target and an expected vehicle perilune of 46 km. The brightness distribution of the target model was represented by two neighboring areas with an average photometric value of the bright and dark side of the cone. Because equation (25) is linear, the rule of superposition allows the two areas to be handled as separate inputs to the camera system and to be combined again at the output. Thus, the peak output signal of each area, $S_{rp}(g,t,s)$ and $S_{qp}(g,t,s)$, can be determined and later combined to yield the desired peak-to-peak output signal

$$S_{p-p}(g,t,s) = S_{rp}(g,t,s) + S_{qp}(g,t,s)$$

It is mathematically convenient to locate the X,Y coordinate axis in such a manner that the signal area is symmetric around it. The signal content of, say, $\Delta E_r(x,g;g,t)$ is then averaged over an area bounded by $-x_0 \leqq x \leqq x_0$ and $-y_0 \leqq y \leqq y_0$. When this two-dimensional exposure level passes through an imaging system which is relatively free from optical aberrations and distortions, maximum light intensity occurs at the center of the resulting image. That is, peak signal occurs where x_0 and y_0 approach zero.

$$S_{rp}(g,t,s) = \frac{\Delta T}{\Delta E}\left(E_b\right) \lim_{\substack{x_0 \to 0 \\ y_0 \to 0}} \frac{1}{4x_0 y_0} \int_{-y_0}^{y_0} \int_{-x_0}^{x_0} \int_{-\infty}^{\infty} \int_{-\infty}^{\infty} \Delta E_r(u,v;g,t)\, G_{l,f,s}(u,v;s)\, e^{i2\pi(ux+vy)} dv\, du\, dx\, dy \qquad (26)$$

Integrating with respect to x and y, and applying the limits, the peak signal becomes

$$S_{rp}(g,t,s) = \frac{\Delta T}{\Delta E}\left(E_b\right) \lim_{\substack{x_0 \to 0 \\ y_0 \to 0}} \int_{-\infty}^{\infty} \int_{-\infty}^{\infty} \Delta E_r(u,v;g,t)\, G_{l,f,s}(u,v;s)\, \frac{\sin 2\pi x_0 u}{2\pi x_0 u}\, \frac{\sin 2\pi y_0 v}{2\pi y_0 v}\, du\, dv$$

$$= \frac{\Delta T}{\Delta E}\left(E_b\right) \int_{-\infty}^{\infty} \int_{-\infty}^{\infty} \Delta E_r(u,v;g,t)\, G_{l,f,s}(u,v;s) du\, dv \qquad (27)$$

The peak signal value of the dark area may be found similarly and added to expression (27) to yield a peak-to-peak signal

$$S_{p-p}(g,t,s) = \frac{\Delta T}{\Delta E}(E_b) \int_{-\infty}^{\infty} \int_{-\infty}^{\infty} \Delta E(u,v;g,t) \, G_{l,f,s}(u,v;s) du \, dv \tag{28}$$

where

$$\Delta E(u,v;g,t) = \Delta E_r(u,v;g,t) + \Delta E_q(u,v;g,t)$$

The integral in the above equation presents a summation of the product of input signal frequency spectrum and system MTF. A film readout aperture scan across the film image transduces the two-dimensional distribution to a one-dimensional function. It is apparent that maximum signal will result if scanning occurs along sunline as illustrated in figure 2(d). In pursuit of a simple to evaluate, approximate expression, a continuous square wave is considered rather than the isolated square-wave pulse. Of the resulting discrete frequency spectrum, the fundamental frequency component k is selected to estimate peak-to-peak signal values as indicated

$$S_{p-p}(g,t,s) = \Delta E(g,t) \, G_{l,f,s}(k;s) \frac{\Delta T}{\Delta E}(E_b) \tag{29}$$

Adding the noise term of equation (17), an approximate expression of the image signal-to-noise ratio becomes

$$\frac{S_{p-p}}{N}(g,t,s) = \Delta E(g,t) \, G_{l,f,s}(k;s) \sqrt{\frac{A_i}{A_a}} \, \frac{\Delta T/\Delta E}{\sigma}(E_b) \tag{30}$$

Change of exposure is related to the average bright and dark photometric value of the cone for a given exposure time (see eq. (24) and table I) by

$$\Delta E(g,t) = \frac{K\rho\pi t}{4f_n^2} \Delta \bar{\Phi}(g) = 690 t\rho \, \Delta \bar{\Phi}(g) \tag{31}$$

The quantity $\Delta \bar{\Phi}(g)$ is given in figure 5. The approximate cone model area (depicted in fig. 2(c)) is

$$A_i = 2\left(\frac{\pi}{4}\right)\left(\frac{d}{2}\right)^2 = 0.39 d^2 \, m^2 \tag{32}$$

The scanning aperture area referred to the lunar surface, using the scaling factor given previously, is

$$A_a = \left(\frac{\pi}{4}\right)\left(\frac{6.48}{13.2}\right)^2 = 0.19 \, m^2 \tag{33}$$

16

And the fundamental cone frequency is

$$k = \frac{1 \text{ line}}{0.0132d \text{ mm}} = \frac{76}{d} \frac{\text{lines}}{\text{mm}}$$ (34)

Finally, substituting equations (31) to (34) into equation (30), and considering that a peak-to-peak signal-to-noise ratio of 3 has been specified as detection threshold, a relation for the minimum detectable cone diameter can be written as

$$3 = \left[690 t\rho \; \Delta\bar{\Phi}(g)\right]\left(\sqrt{\frac{0.39d^2}{0.19}}\right)\left[G_{l,f,s}\left(\frac{76}{d};s\right)\right]\left[\frac{\Delta T/\Delta E}{\sigma}(E_b)\right]$$ (35)

Grouping exposure- and phase-angle-dependent parameters on the left side of the equality sign and the frequency-dependent parameters on the right side, the equation becomes

$$\frac{0.003}{t\rho \; \Delta\bar{\Phi}(g)\frac{\Delta T/\Delta E}{\sigma}(E_b)} = d \; G_{l,f,s}\left(\frac{76}{d};s\right)$$ (36)

This equation has to be solved for d by trial and error. Solutions for exposure times of 1/25 and 1/50 second and a lunar albedo of 0.07 are plotted in figure 8. In one case, image smear is assumed to be absent; in the other case, smear rate is assumed to be a 1σ value of 10 meters/second (ref. 16).

Expected value of minimum detectable cone diameter.- The expected value of the minimum detectable cone diameter can be found approximately from the results given in figure 8 by using a numerical summation for equation (19) as follows:

$$\langle d_{min} \rangle = \sum_{j=1}^{m} \sum_{i=1}^{n} d_{min}\left(\log E_i, g_j\right) p\left(\log E_i/g_j\right) p\left(g_j\right)$$ (37)

Exposure is replaced by log exposure for convenience as pointed out previously.

The accuracy of these summations depends, of course, on the number of intervals used. $\langle d_{min} \rangle$ is calculated here for $n = 5$ and $m = 7$ intervals ranging between the 3σ values of exposure and phase angle as depicted in figure 4. Results of these calculations are shown in figure 9.

Confidence levels in detection of a specified cone diameter.- Confidence levels in the detection of specified cone diameters can be found by using equation (23) and the results of equation (37). Again, it is easier to work with log exposure instead of exposure. Results of these calculations for a specified 2-meter-diameter cone at no image smear and at a smear rate of 10 meters/second are shown in figures 10(a) and 10(b), respectively. Assuming that a shutter speed of 1/25 second is used for $g > 74^O$ and of

17

1/50 second for $g < 74^\circ$, the confidence levels in detecting 2-, 3-, and 4-meter-diameter cones at the image smear rate of 10 meters/second are plotted in figure 11.

Discussion of Results

Several factors of primary importance may be noted from the results of these calculations.

(1) As shown in figure 8(a), best picture quality in revealing small lunar detail occurs at high phase angles (70° to 83° for a lunar albedo of 0.07) and long exposure times (1/25 second) if image smear is negligible. Furthermore, picture quality degrades rapidly at phase angles above 83° and slowly below 70°. In the presence of some image smear, as shown in figure 8(b), shorter exposure times (1/50 second) and, therefore, lower phase angles (62° to 74°) are preferable.

(2) Curves depicting the variation of minimum detectable cone diameters with changes in phase angle (fig. 8) and those depicting its average value (fig. 9) differ in proportion to the rate of degradation with changes in exposure and phase angle and the magnitude of uncertainties in exposure and phase angle.

(3) While a cone of 2-meter-diameter may be detected in a range of phase angles extending from 51° to 86° (fig. 8(a)) for a vehicle perilune of 46 kilometers, in the absence of image smear, and under expected conditions in lunar reflection and vehicle performance, confidence levels in the detection of cones this size decrease rapidly below 0.5 outside the range of 54° to 85° (fig. 10(a)).

(4) Final results are summarized in figure 11. Shown are the variations of confidence levels in the detection of 2-, 3-, and 4-meter-diameter cones with phase angle. Trade-offs in phase angle (trajectory) design are readily apparent between low confidence levels in the detection of small detail and higher and wider confidence bands in the detection of larger detail.

CONCLUDING REMARKS

An analysis is presented which relates photographic quality in revealing small lunar detail to viewing geometry and film exposure and hence to mission controllable parameters. Results of this analysis show that the best performance can be achieved for Lunar Orbiter's vertical photography at high phase angles and slow shutter speeds providing that no error exists in the lunar photometric model and no deviation occurs from the expected vehicle operation.

To consider uncertainties in lunar reflectance and system operation, a strategy is developed which permits the selection of vehicle trajectories and camera shutter speeds

18

for optimum confidence levels in achieving a specified performance. Application of this strategy leads to the selection of a range of phase angles extending from 65° to 80° as giving the highest level of confidence in the detection of 2-meter-diameter cones. A low and narrow confidence band in the detection of small lunar detail can be traded for a higher and wider confidence band in the detection of larger detail by small vehicle trajectory changes.

Langley Research Center,
    National Aeronautics and Space Administration,
        Langley Station, Hampton, Va., June 26, 1967,
        814-11-00-03-23.

APPENDIX

CALCULATION OF AN AVERAGE PHOTOMETRIC VALUE FOR THE
BRIGHT AND DARK SIDE OF A LUNAR CONE

The average photometric function of the bright and dark halves of a lunar cone depends on phase angle g and an effective lunar slope β_e. This slope is measured around the right-circular cone as a function of the angle θ away from the plane formed by the incident sun and the camera as depicted in figures 2 and 12 and may be written in terms of the coordinate variables as

$$\beta_e(\theta) = -\tan^{-1}\left[\frac{dz}{dy}(\theta)\right] \tag{A1}$$

The equation for a right-circular cone is

$$x^2 + y^2 = \frac{z^2}{c^2} \tag{A2}$$

where c is a constant. Solving this equation for z and differentiating with respect to y yields

$$z = c\left(x^2 + y^2\right)^{1/2} \tag{A3}$$

$$\frac{dz}{dy} = \frac{cy}{\left(x^2 + y^2\right)^{1/2}} \tag{A4}$$

Substituting $x = \sin\theta$ and $y = \cos\theta$ into equation (A4) gives

$$\frac{dz}{dy} = c\cos\theta \tag{A5}$$

When $\theta = 0$,

$$\frac{dz}{dy} = \frac{2h}{d}$$

where h is the cone height and d is the base diameter. Thus,

$$\frac{dz}{dy} = \frac{2h}{d}\cos\theta \tag{A6}$$

The effective slope is, therefore,

$$\beta_e = -\tan^{-1}\left[\frac{2h}{d}\cos\theta\right] \tag{A7}$$

APPENDIX

For a 26.6° cone, which has a base-to-height ratio of 4:1, this becomes

$$\beta_e = -\tan^{-1}\left[0.5 \cos \theta\right] \tag{A8}$$

The average photometric function of the bright half of the cone $\bar{\Phi}_r(g)$ and the dark half $\bar{\Phi}_q(g)$ may now be obtained from the photometric curves as indicated

$$\bar{\Phi}_r(g) = \frac{1}{n} \sum_{i=0}^{n} \Phi_i(g, \beta_e) \qquad (-90^\circ < \theta_i < 90^\circ) \tag{A9a}$$

$$\bar{\Phi}_q(g) = \frac{1}{n} \sum_{i=0}^{n} \Phi_i(g, \beta_e) \qquad (90^\circ < \theta_i < 270^\circ) \tag{A9b}$$

Results of this averaging for $n = 19$ (10° intervals) is shown in figure 5.

REFERENCES

1. Fellgett, P. B.; and Linfoot, E. H.: On the Assessment of Optical Images. Phil. Trans. Roy. Soc. London, ser. A, vol. 247, no. 931, Feb. 17, 1955, pp. 369-407.

2. Herriman, A. G.; Washburn, H. W.; and Willingham, D. E.: Ranger Preflight Science Analysis and the Lunar Photometric Model. Tech. Rept. No. 32-382 (Rev.) (Contract No. NAS 7-100), Jet Propulsion Lab., California Inst. Technol., Mar. 11, 1963.

3. Hapke, Bruce W.: A Theoretical Photometric Function for the Lunar Surface. J. Geophys. Res., vol. 68, no. 15, Aug. 1, 1963, pp. 4571-4586.

4. Willingham, D.: The Lunar Reflectivity Model for Ranger Block III Analysis. Tech. Rept. No. 32-664 (Contract No. NAS 7-100), Jet Propulsion Lab., California Inst. Technol., Nov. 2, 1964.

5. Keene, George T.: Lunar Photo Study. Z-3841 (Contract NAS9-3826), Eastman Kodak Co., Oct. 1, 1965.

6. Linfoot, E. H.: Fourier Methods in Optical Image Evaluation. The Focal Press, c.1964.

7. Jones, R. Clark: On the Point and Line Spread Functions of Photographic Images. J. Opt. Soc. Am., vol. 48, no. 12, Dec. 1958, pp. 934-937.

8. Scott, Roderic M.: Contrast Rendition as a Design Tool. Phot. Sci. Eng., vol. 3, no. 5, Sept.-Oct. 1959, pp. 201-209.

9. Kinzly, R. E.; Roetling, P. G.; and Holladay, T. M.: Project SLOPE — Study of Lunar Orbiter Photographic Evaluation. Rept. No. VS-2182-D-2 (NASA CR-66158), Cornell Aeron. Lab., Inc., May 20, 1966.

10. Rindfleisch, T.; and Willingham, D.: A Figure of Merit Measuring Picture Resolution. Tech. Rept. No. 32-666 (Contract No. NAS 7-100), Jet Propulsion Lab., California Inst. Technol., Sept. 1, 1965.

11. Brock, G. C.: Microimage Quality. Photographic Considerations for Aerospace, H. J. Hall and H. K. Howell, eds., Itek Corp., c.1965, pp. 42-72.

12. O'Neill, Edward L.: Introduction to Statistical Optics. Addison-Wesley Pub. Co., Inc., c.1963, p. 113.

13. Brunk, H. D.: An Introduction to Mathematical Statistics. Ginn and Co., c.1960, p. 157.

14. Schade, Otto H., Sr.: An Evaluation of Photographic Image Quality and Resolving Power. J. SMPTE, vol. 73, no. 2, Feb. 1964, pp. 81-119.

15. Rose, Albert: The Sensitivity Performance of the Human Eye on an Absolute Scale. J. Opt. Soc. Am., vol. 38, no. 2, Feb. 1948, pp. 196-208.

16. Anon.:   Photographic Subsystem Reference Handbook for the Lunar Orbiter Program. L-018375-RU, Eastman Kodak Co., Mar. 15, 1966.

17. Hoel, Paul G.:   Introduction to Mathematical Statistics.   Second ed., John Wiley & Sons, Inc., c.1954, p. 204.

18. Electron. Technol.:   Picture Data Systems Analysis.   Doc. No. D2-100293-1 (Contract No. NAS 1-3800), Boeing Co., Dec. 1964.

19. Wolf, Jack K.; and Thomas, John B.:   On the Recognition of Signal Patterns in Noise. RADC-TN-61-83, U.S. Air Force, May 1961.

TABLE I.- NOMINAL VALUES AND TOLERANCES

Functions	Nominal values	3σ exposure	3σ log exposure
Solar constant, K	1.3×10^5 meter-candles	------	----
Static lens transmission, τ	0.66	------	----
f-number, f_n	5.6	------	----
Phase angle, g	0° - 90°, ($\pm 3.5^O$, 3σ)	------	----
Film	See figure 9	$\approx \pm 23\%$	0.10
Shutter time (static), t	1/25 and 1/50 sec	$\pm 25\%$	.11
Shutter time (dynamic), t	1/25 and 1/50 sec	$\pm 5\%$	.02
Lunar albedo, ρ	0.05 - 0.13	$\pm 40\%$	.17
Photometric function, Φ	See figure 3	$\pm 30\%$	.13
Exposure, E	rss	$\pm 64\%$	0.28
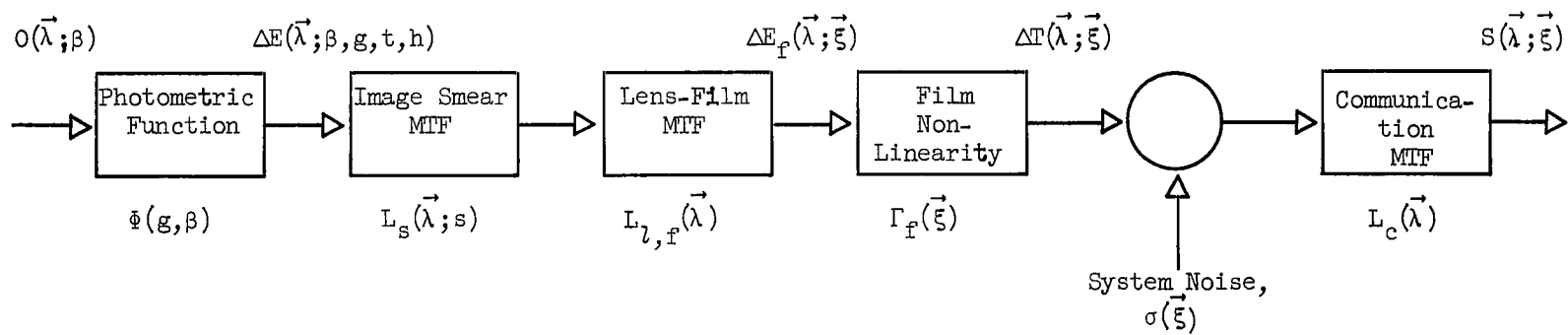
Figure 1.- Block diagram of Lunar Orbiter photographic system.

$O(\vec{\lambda};\beta)$ $\Delta E(\vec{\lambda};\beta,g,t,h)$ $\Delta E_f(\vec{\lambda};\vec{\xi})$ $\Delta T(\vec{\lambda};\vec{\xi})$ $S(\vec{\lambda};\vec{\xi})$

Photometric Function   Image Smear MTF   Lens-Film MTF   Film Non-Linearity   Communication MTF

$\Phi(g,\beta)$ $L_s(\vec{\lambda};s)$ $L_{\ell,f}(\vec{\lambda})$ $\Gamma_f(\vec{\xi})$ $L_c(\vec{\lambda})$

System Noise, $\sigma(\vec{\xi})$
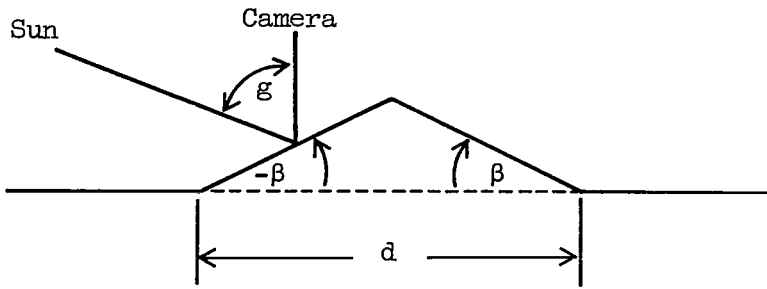
(a) Viewing geometry and side view of cone.
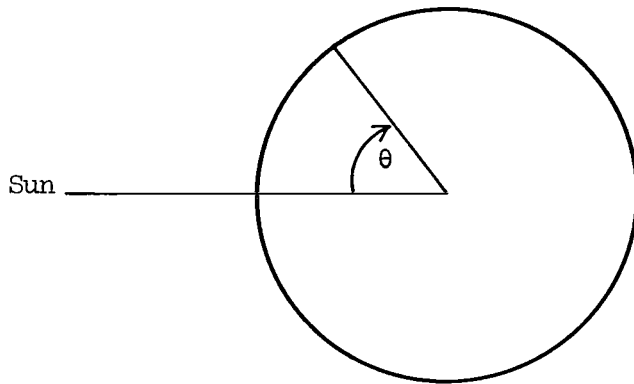
(b) Top view of cone.
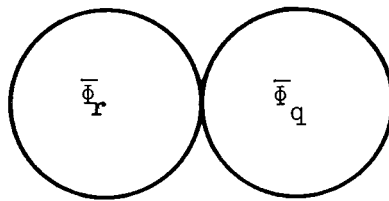
(c) Top view of cone model.
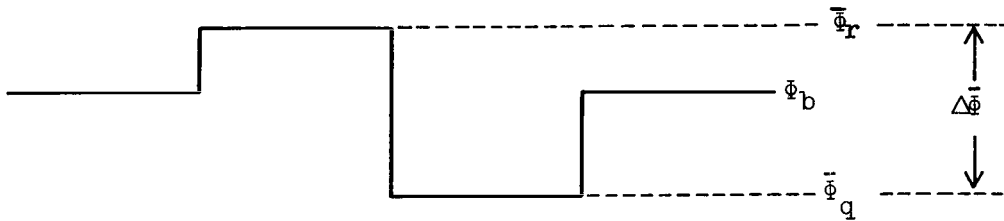
(d) One-dimensional approximation of cone model.

Figure 2.- Lunar Orbiter viewing geometry and lunar cone model.

26
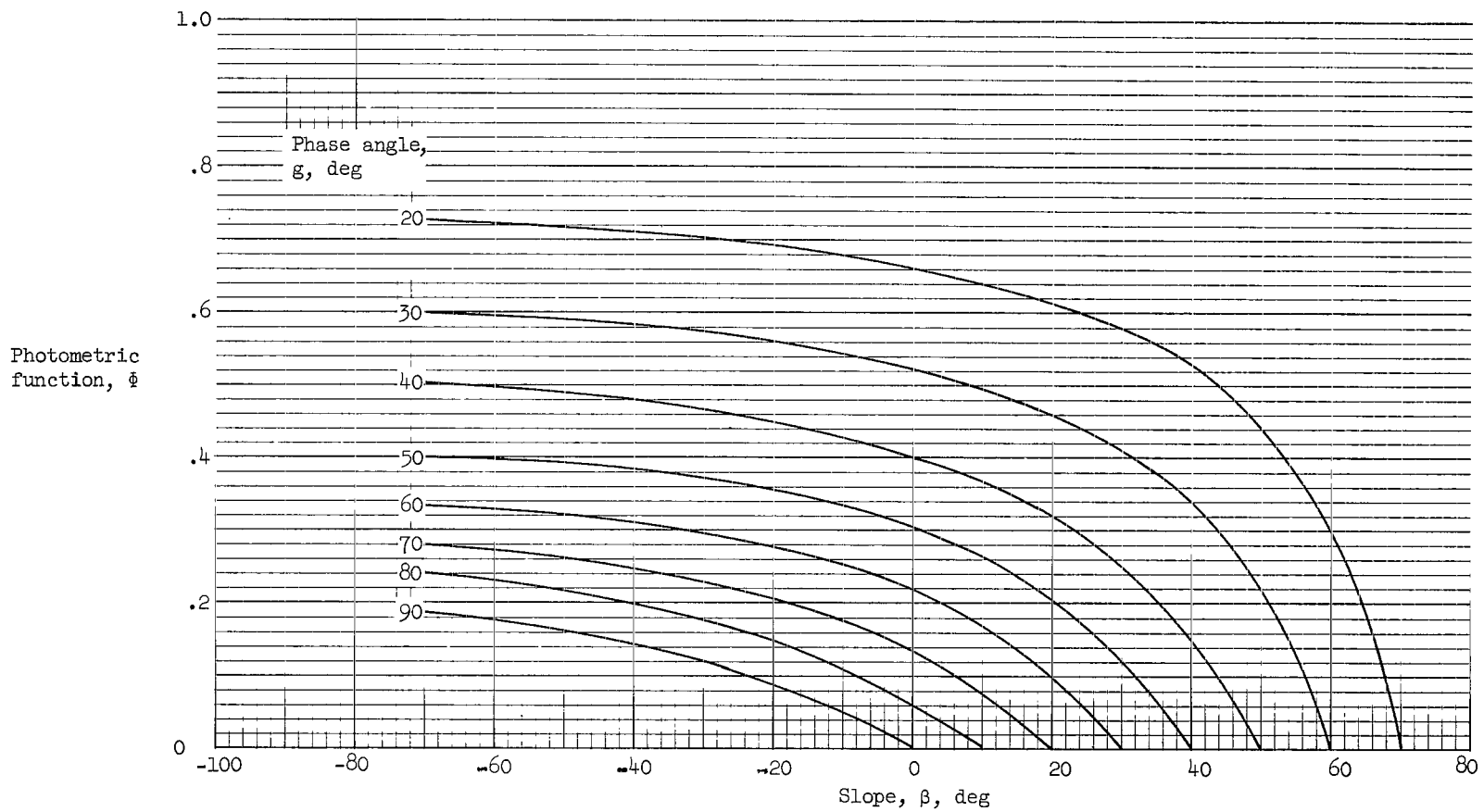
Figure 3.- Photometric function of lunar surface.
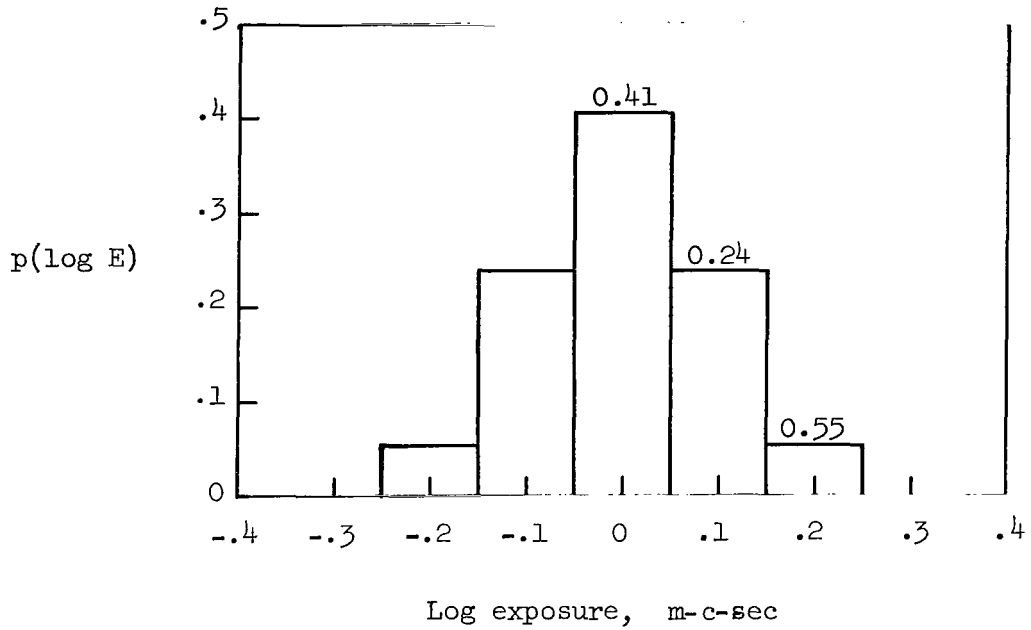
(a) Log exposure probability distribution, $3\sigma = \pm0.28$.
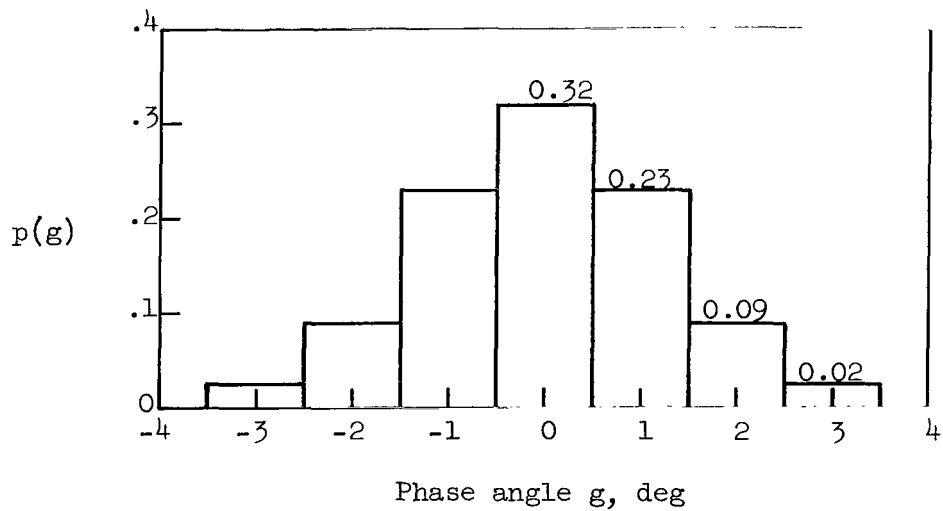
(b) Phase angle probability distribution, $3\sigma = \pm3.5°$.

Figure 4.- Gaussian log exposure and phase angle probability distribution approximated over discrete intervals.
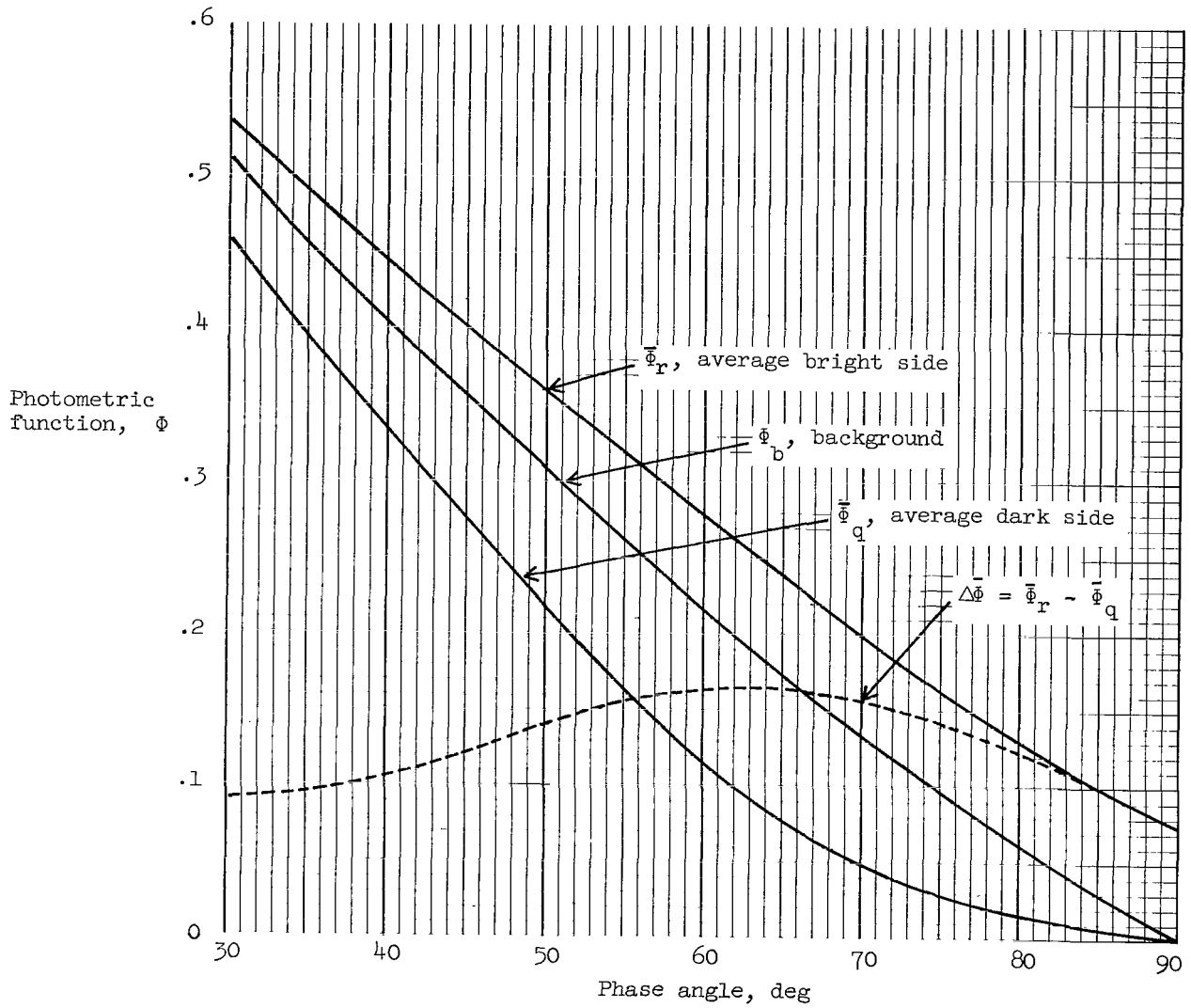
Figure 5.- Average photometric function of bright side $\bar{\Phi}_r$ and dark side $\bar{\Phi}_q$ of a 26.6° cone and their difference $\Delta\bar{\Phi}$.
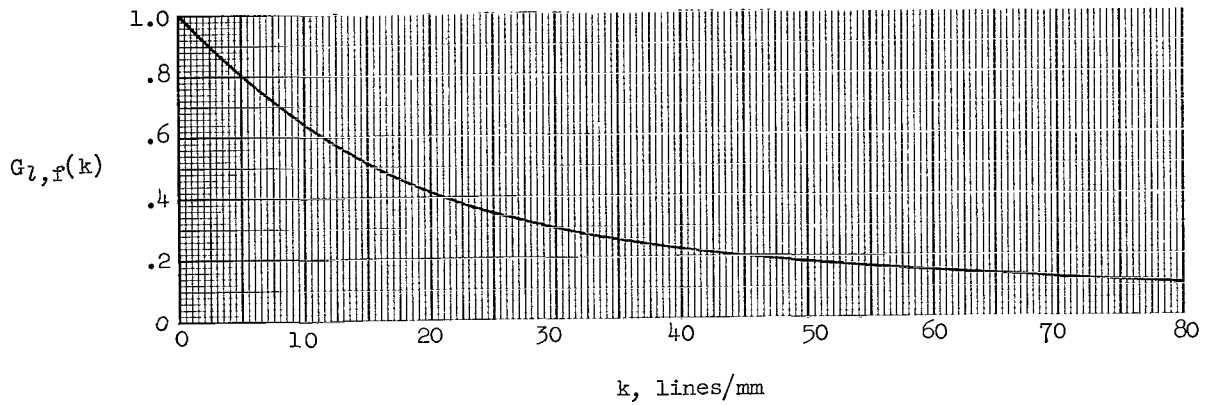
(a) Modulation transfer function for lens and film.

| Curve | Image smear σ | |
	film, mm	moon, m
1	0.0026	0.2
2	0.0052	0.4
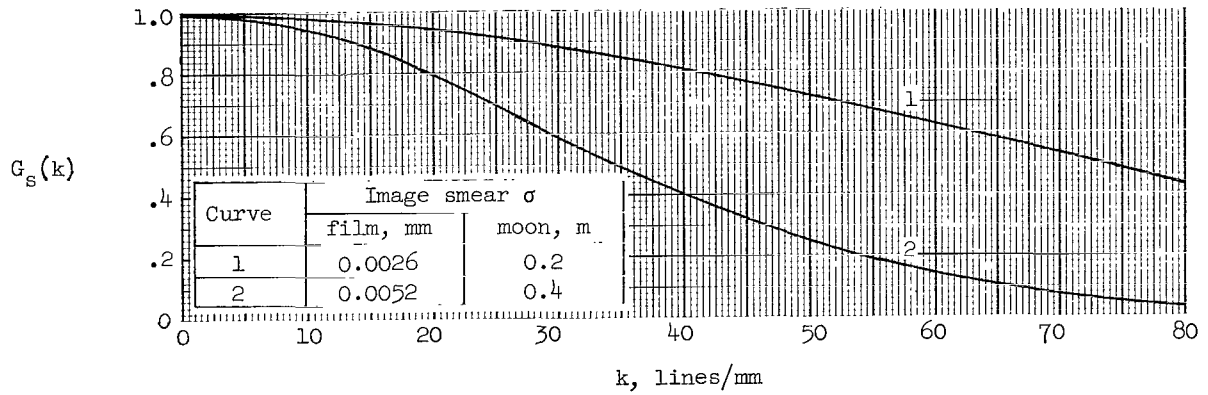
(b) Modulation transfer function for image smear.

| Curve | Smear rate, m/sec | |
	t = 1/25	t = 1/50
1	5	10
2	10	20
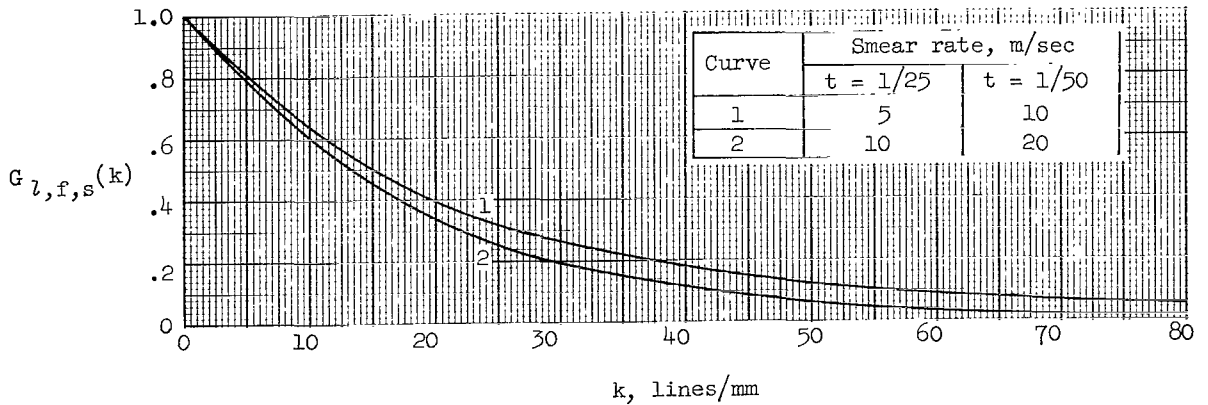
(c) Combined modulation transfer function for lens, film, and image smear.

Figure 6.- Modulation transfer functions for photographic subsystem and image smear. Smear is assumed Gaussian and is designated by its standard deviation referred to the film image and to the lunar surface for a vehicle perilune of 46 km.

(a) Film transmission plotted against exposure.

$$\sigma = (\sigma_T^2 + \sigma_c^2)^{1/2}$$
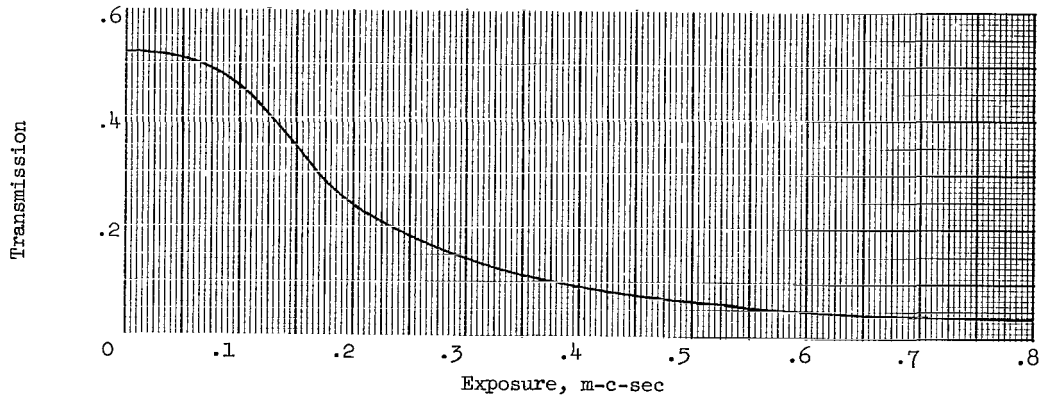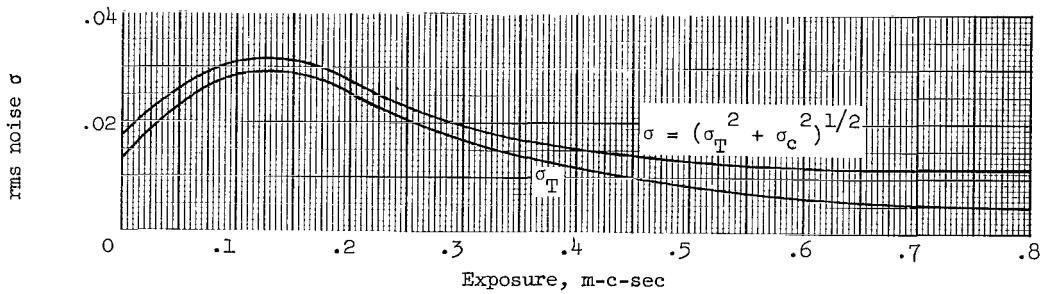
(b) Film transmission noise and total system noise plotted against exposure.
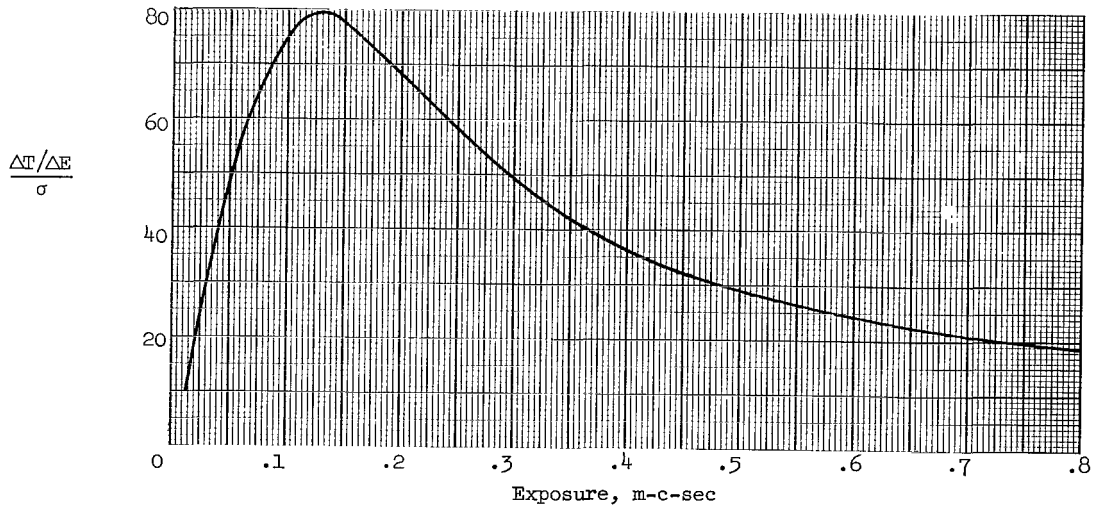
(c) Film-sensitivity-to-rms-system-noise ratio plotted against exposure.

Figure 7.- Exposure-dependent transfer functions for the photographic subsystem. Communications signal-to-noise ratio, 30 dB.
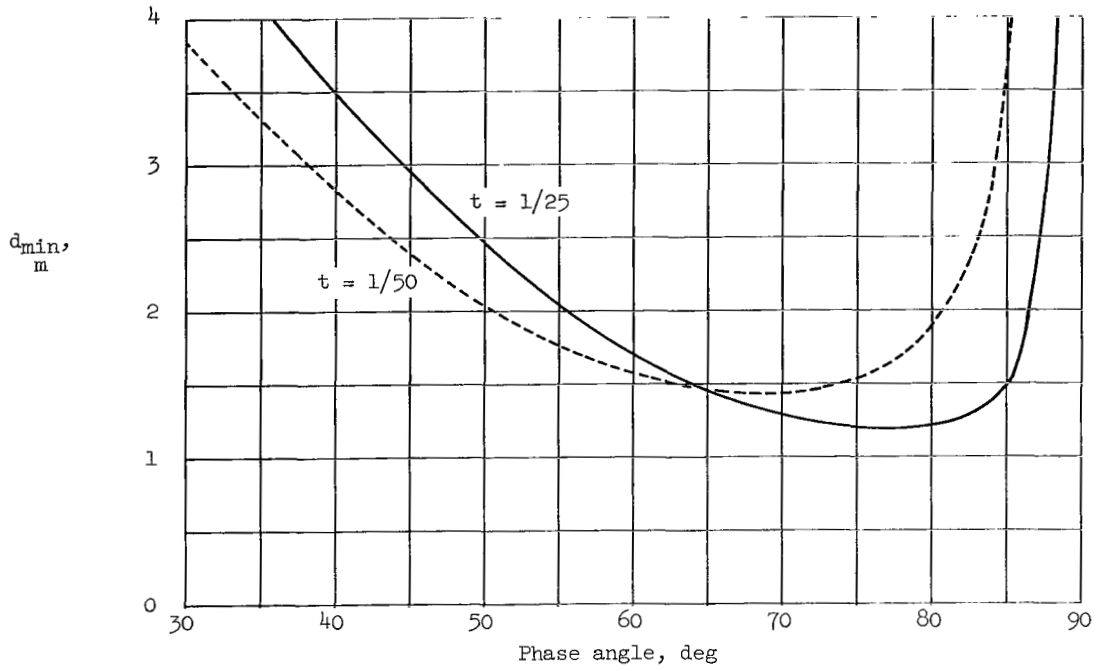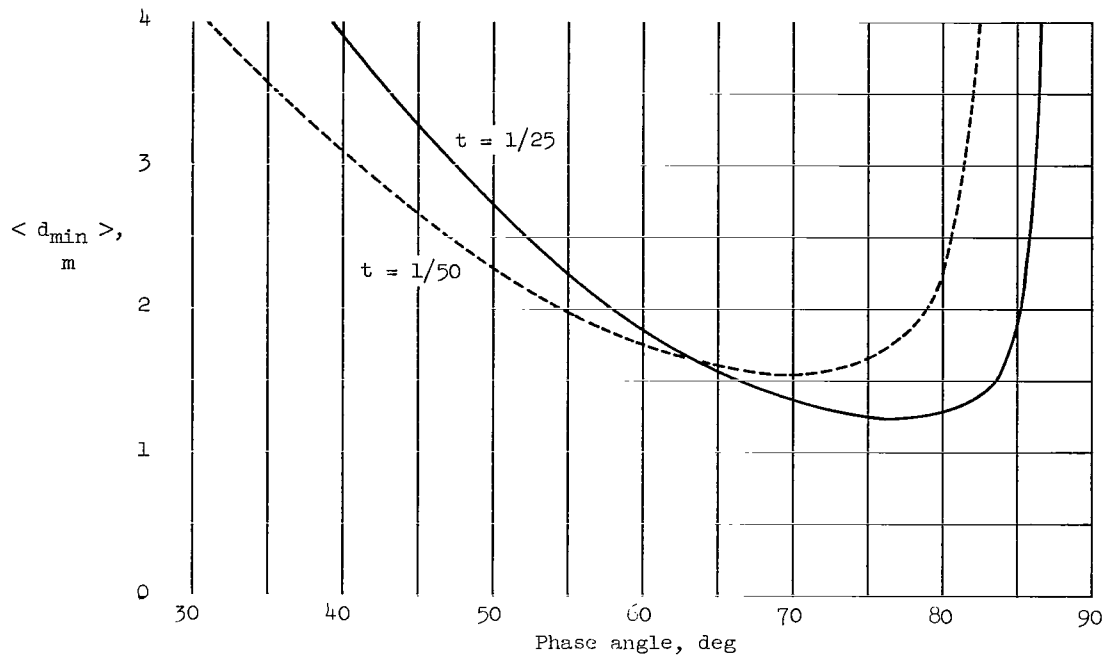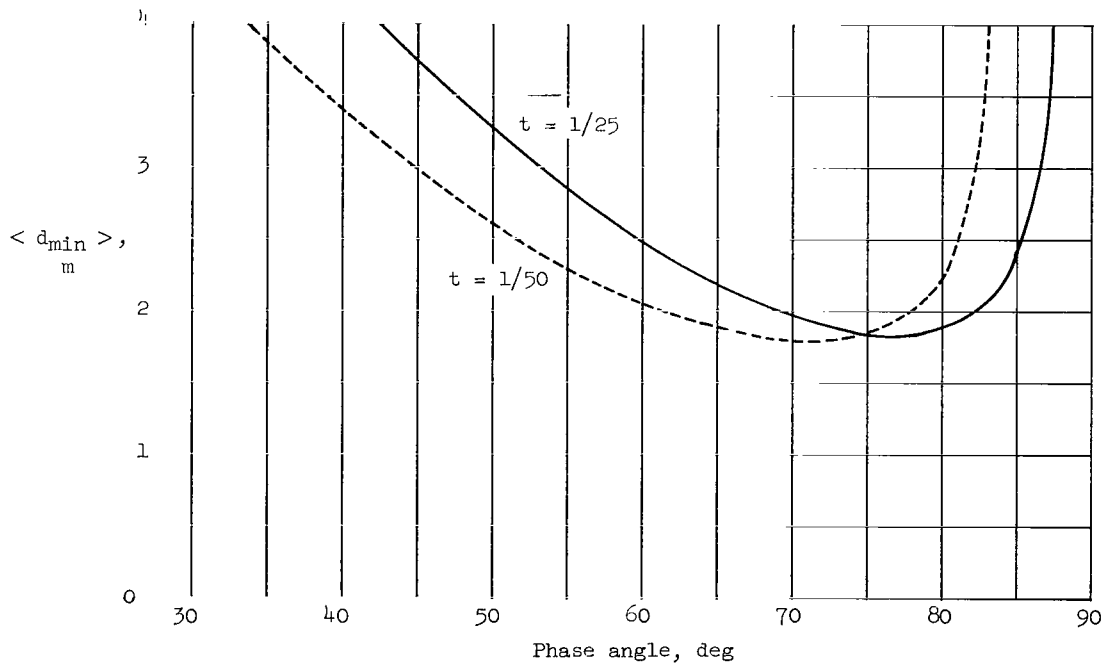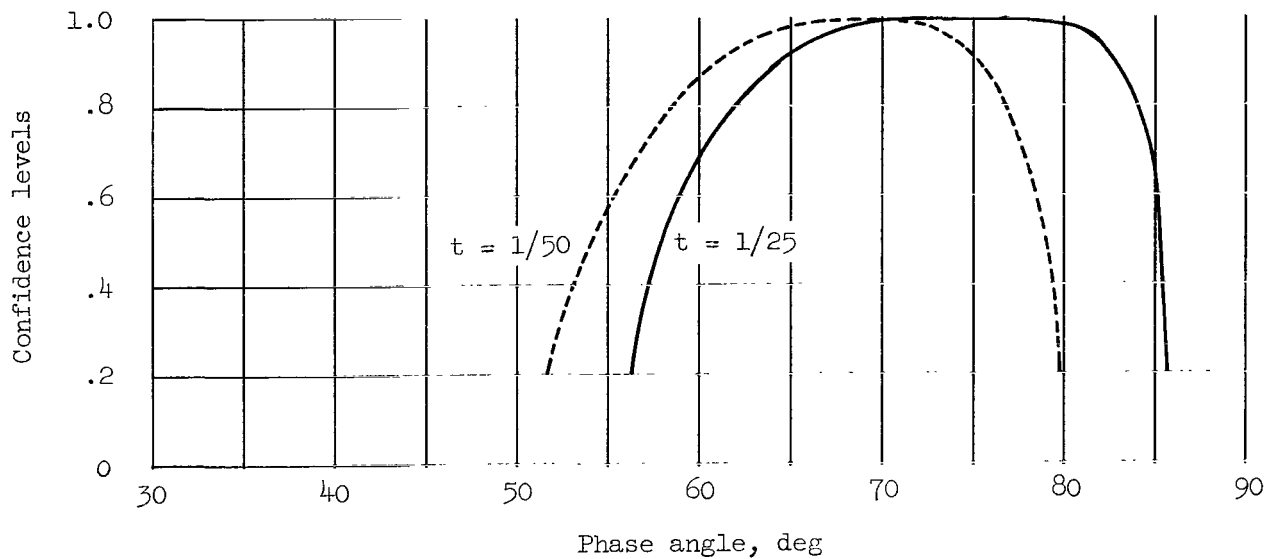
(a) Image smear absent.
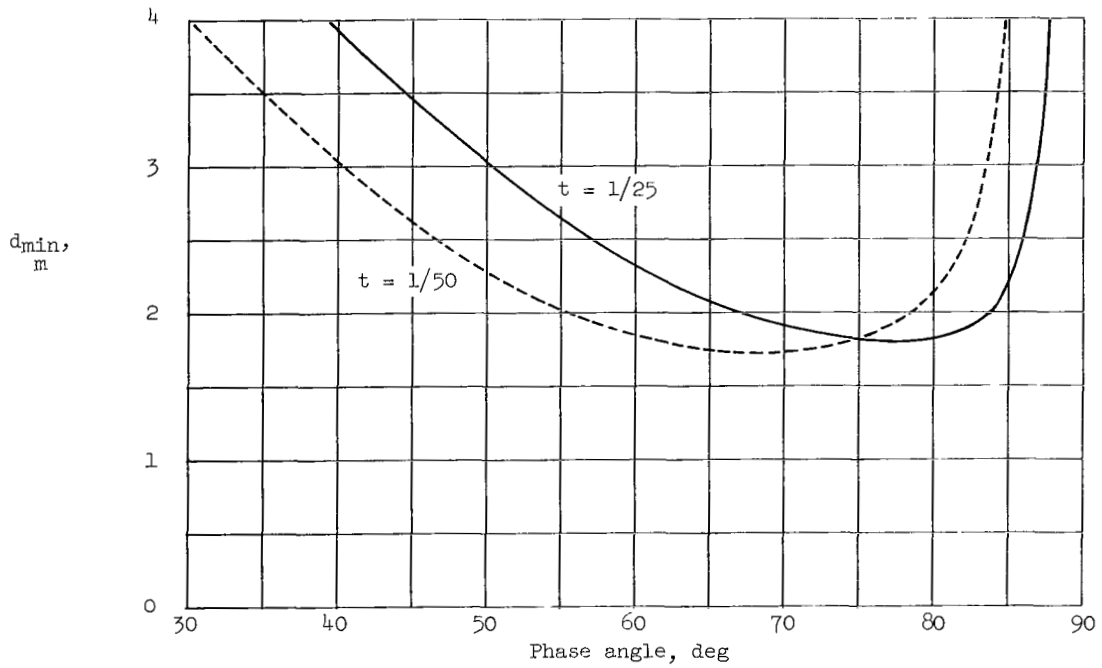
(b) Image smear rate, 10 meters/second.

Figure 8.- Variation of minimum detectable 26.6° cone diameter with phase angle. Image smear is assumed Gaussian and is designated by its standard deviation referred to the lunar surface for a vehicle perilune of 46 km. Lunar albedo, 0.07.
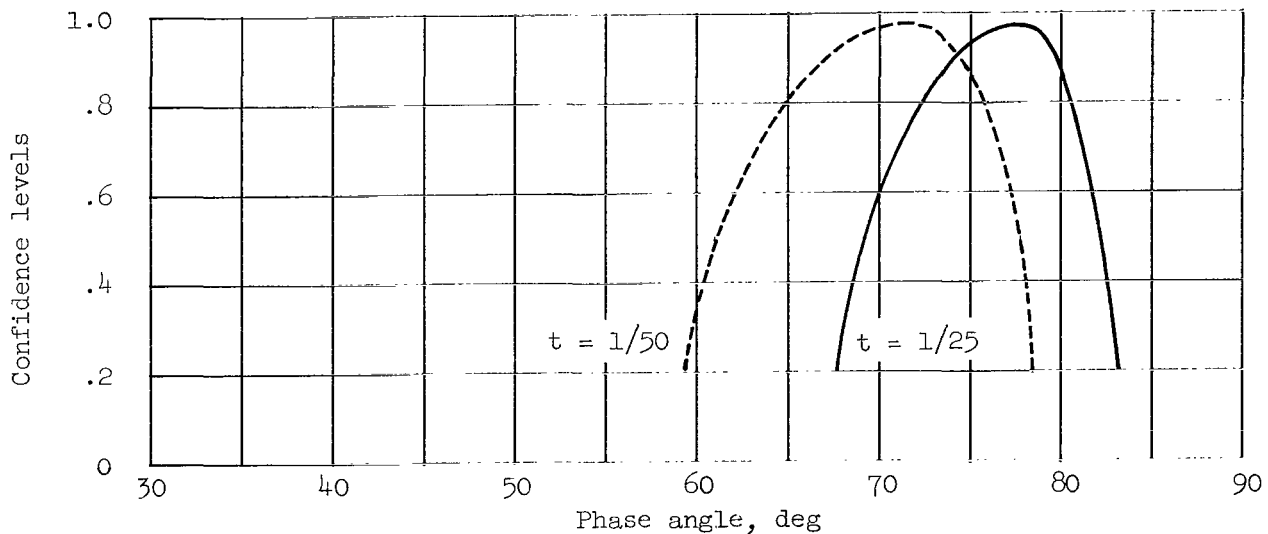
(a) Image smear absent.

(b) Image smear rate, 10 meters/second.

Figure 9.- Variation of expected value of the minimum detectable 26.6° cone diameter with phase angle. Image smear is assumed Gaussian and is designated by its standard deviation referred to the lunar surface for a vehicle perilune of 46 km. Lunar albedo, 0.07.
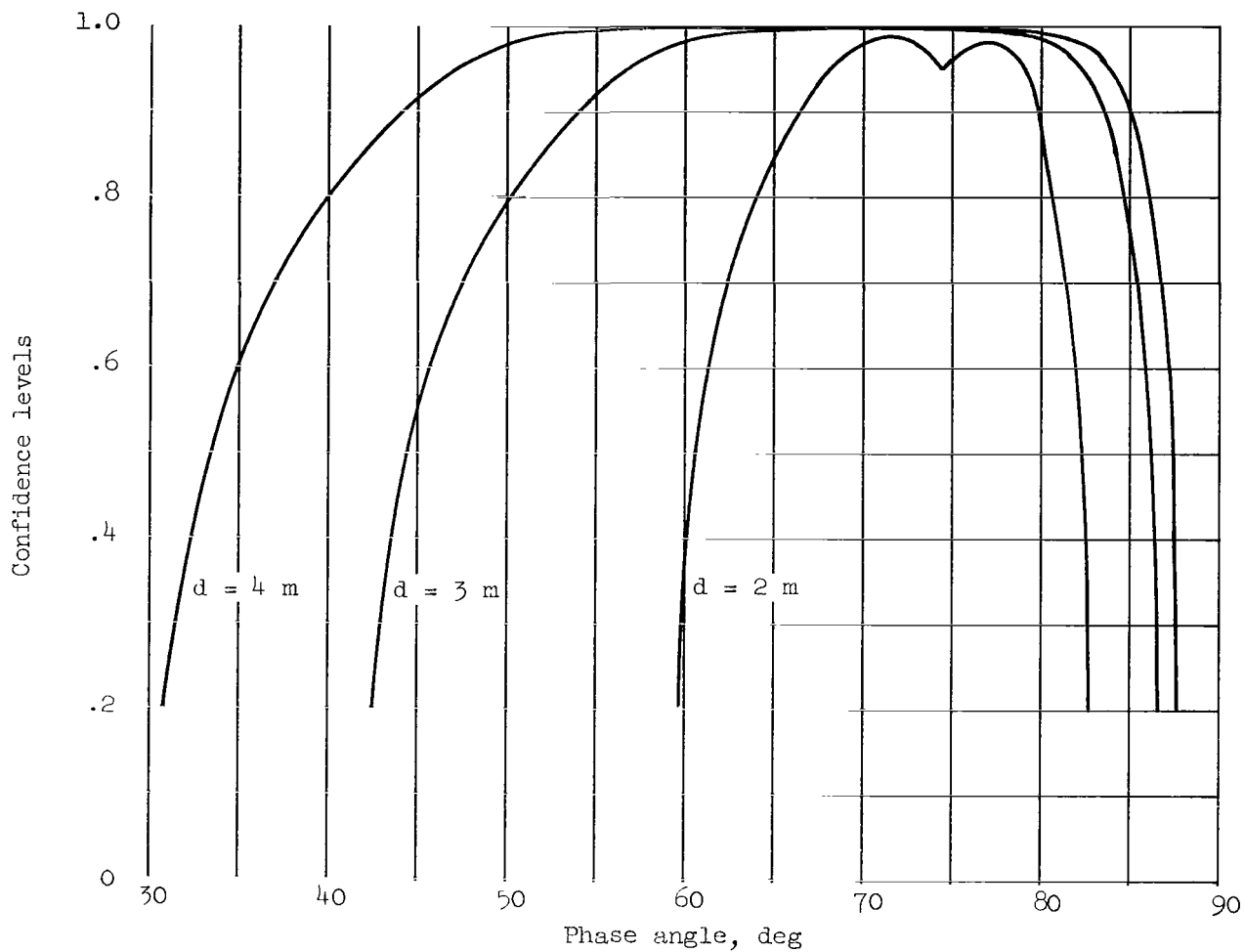
(a) Image smear absent.

(b) Image smear rate, 10 meters/second.

Figure 10.- Variation of confidence levels in the detection of 2-meter-diameter, 26.6° cones with phase angle. Image smear is assumed Gaussian and is designated by its standard deviation referred to the lunar surface for a vehicle perilune of 46 km. Lunar albedo, 0.07.

34

Figure 11.- Variation of confidence levels in the detection of 2-, 3-, and 4-meter-diameter, 26.6° cones with phase angle. Image smear is assumed Gaussian and its standard deviation, referred to the lunar surface for a vehicle perilune of 46 km, is 10 meters/second. Exposure time is 1/25 sec at g > 74° and 1/50 sec at g < 74°; lunar albedo, 0.07.
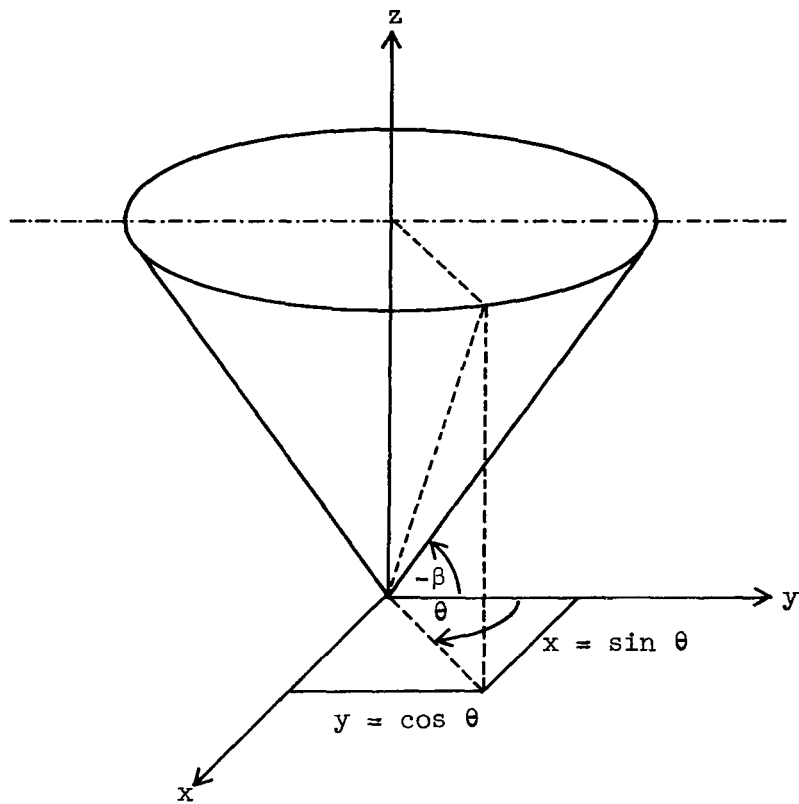
Figure 12.- Cone geometry.

L-5465

*"The aeronautical and space activities of the United States shall be
conducted so as to contribute . . . to the expansion of human knowl-
edge of phenomena in the atmosphere and space. The Administration
shall provide for the widest practicable and appropriate dissemination
of information concerning its activities and the results thereof."*

— NATIONAL AERONAUTICS AND SPACE ACT OF 1958

NASA SCIENTIFIC AND TECHNICAL PUBLICATIONS

TECHNICAL REPORTS: Scientific and
technical information considered important,
complete, and a lasting contribution to existing
knowledge.

TECHNICAL NOTES: Information less broad
in scope but nevertheless of importance as a
contribution to existing knowledge.

TECHNICAL MEMORANDUMS:
Information receiving limited distribution
because of preliminary data, security classifica-
tion, or other reasons.

CONTRACTOR REPORTS: Scientific and
technical information generated under a NASA
contract or grant and considered an important
contribution to existing knowledge.

TECHNICAL TRANSLATIONS: Information
published in a foreign language considered
to merit NASA distribution in English.

SPECIAL PUBLICATIONS: Information
derived from or of value to NASA activities.
Publications include conference proceedings,
monographs, data compilations, handbooks,
sourcebooks, and special bibliographies.

**TECHNOLOGY UTILIZATION
PUBLICATIONS**: Information on technology
used by NASA that may be of particular
interest in commercial and other non-aerospace
applications. Publications include Tech Briefs,
Technology Utilization Reports and Notes,
and Technology Surveys.

Details on the availability of these publications may be obtained from:

SCIENTIFIC AND TECHNICAL INFORMATION DIVISION

NATIONAL AERONAUTICS AND SPACE ADMINISTRATION
Washington, D.C. 20546